Simulation of Co-Existence of Ballooning and Kink Instabilities in PLATO Tokamak Plasma

Shuhei TOMIMATSU[1)], Naohiro KASUYA[1,2)], Masahiko SATO[3)], Atsushi FUKUYAMA[4)], Masatoshi YAGI[5)], Yoshihiko NAGASHIMA[1,2)] and Akihide FUJISAWA[1,2)]

[1)]*Interdisciplinary Graduate School of Engineering Sciences, Kyushu University, Kasuga, Fukuoka 816-8580, Japan*
[2)]*Research Institute for Applied Mechanics, Kyushu University, Kasuga, Fukuoka 816-8580, Japan*
[3)]*National Institute for Fusion Science, Toki, Gifu 509-5292, Japan*
[4)]*Department of Nuclear Engineering, Kyoto University, Nishikyo-ku, Kyoto 615-8540, Japan*
[5)]*National Institute for Quantum and Radiological Science and Technology, Obuchi, Rokkasho-mura, Aomori 039-3212, Japan*

(Received 13 February 2020 / Accepted 2 June 2020)

Magneto-hydro-dynamics (MHD) simulations are carried out for the first time with PLATO tokamak parameters to represent competition of plasma instabilities. The plasma equilibrium is evaluated with the vertical coil configuration in PLATO by using free boundary equilibrium code. The equilibrium is introduced from TASK/EQ to MHD simulations by MIPS code to calculate nonlinear saturation dynamics. In the simulation, a ballooning mode and kink mode both become unstable. We present the dependencies on plasma parameters to identify the instabilities. The ballooning and kink modes become unstable in the steep gradient region and at the safety factor $q = 1$ surface near the center of the plasma, respectively, so the nonlinear flattening of the pressure profile near the center is stronger in the kink case. The interaction between the modes affects the evolution of instabilities.

Keywords: ballooning mode, kink mode, PLATO tokamak, nonlinear dynamics, flattening process

DOI: 10.1585/pfr.15.1403052

1. Introduction

In order to realize a fusion reactor, it is necessary to sustain stable confinement of high-temperature plasmas. However, in a torus plasma, there are various instabilities that have their characteristic spatial-temporal scales (e.g. Magneto-Hydro-Dynamics (MHD), ion and electron scales), and these instabilities make it difficult to confine the plasma [1, 2]. MHD instabilities due to the pressure gradient and the plasma current cause plasma collapse phenomena [3–5]. Nonlinear interactions between electromagnetic modes are important, and small-scale and large-scale modes affect to each other to regulate the saturated states [6]. Therefore, understanding the characteristics of MHD instabilities is essential for stable control of plasma performance.

In order to understand the physical mechanism of plasma dynamical phenomena, laboratory size tokamak PLATO is now under construction in Kyushu university to make detailed measurements of plasma perturbations by using various experimental diagnostics [7]. The flexible design of PLATO tokamak makes it possible to observe dynamics of 3-D turbulence structures. The expected plasma parameters of PLATO tokamak are following; major radius $R = 0.7\,\mathrm{m}$, minor radius $a = 0.2\,\mathrm{m}$, plasma volume $V_P = 0.9\,\mathrm{m}^3$, electron temperature $T_e = 0.2\,\mathrm{keV}$, density $n = 1.0 \times 10^{19}\,\mathrm{m}^3$.

In this study, the target is MHD instabilities with macro scales, and we carry out MHD simulations by using PLATO tokamak parameters to represent dynamics of MHD instabilities in a tokamak plasma. Ballooning and kink modes are induced depending on the safety factor q profile and the steep gradient region, and pressure flattening processes accompanied with competition of instabilities are investigated in the nonlinear dynamics.

2. Equilibrium in PLATO

The plasma equilibria considering the experimental conditions are evaluated by using the module EQU in integrated transport code TASK [8]. TASK/EQU calculates equilibria with free boundary conditions in existence of external vertical coils [9]. Figure 1 shows the magnetic configuration obtained by using the set of external coil currents CASE 1 in Table 1. In this calculation, only D, H and Q coils are used for control parameters. This calculation gives toroidal magnetic field $B_t = 0.3\,\mathrm{T}$, plasma current $I_P = 40\,\mathrm{kA}$, central-beta $\beta_t = 2\%$, central-q $q_{\mathrm{axis}} = 0.7$, surface-q $q_{\mathrm{surf}} = 9.8$, ellipticity $\kappa = 1.6$ triangularity $\delta = 0.3$.

author's e-mail: tomimatsu@riam.kyushu-u.ac.jp

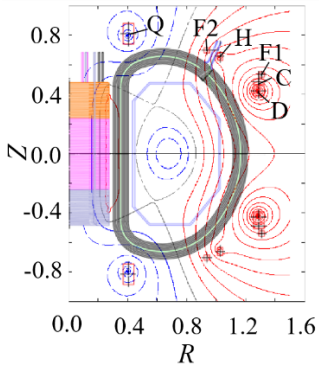

Fig. 1 Magnetic configuration obtained by TASK/EQU for CASE 1 in Table 1. The configuration has up-down symmetry.

Table 1 Set of vertical coil currents used for evaluation (CASE 1). Max represents the maximum limits of the coil currents.

Coil Name	Max(kA turn)	CASE1(kA turn)
OH	134	50
OHC	134	50
D	38	24
Q	76	40
H	14	10
C	-	0
F1	9	0
F2	9	0

3. MHD Simulation

For simulations of MHD instabilities in PLATO tokamak, MIPS code [10] is used. MIPS code solves the MHD equations described below in the cylindrical coordinates (R, Z, ϕ);

$$\rho\frac{\partial\vec{v}}{\partial t} = \rho\vec{\omega}\times\vec{v} - \rho\nabla\left(\frac{v^2}{2}\right) - \nabla p + \vec{j}\times\vec{B} + \frac{4}{3}\nabla\left[\nu\rho(\nabla\cdot\vec{v})\right] - \nabla\times[\nu\rho\vec{\omega}], \quad (1)$$

$$\frac{\partial\rho}{\partial t} = -\nabla\cdot(\rho\vec{v}), \quad (2)$$

$$\frac{\partial\vec{B}}{\partial t} = -\nabla\times\vec{\mathrm{E}}, \quad (3)$$

$$\vec{E} = -\vec{v}\times\vec{\mathrm{B}} + \eta\vec{j}, \quad (4)$$

$$\vec{j} = \frac{1}{\mu_0}\nabla\times\vec{B}, \quad (5)$$

$$\vec{\omega} = \nabla\times\vec{v}, \quad (6)$$

$$\frac{\partial p}{\partial t} = -\nabla\cdot(p\vec{v}) - (\gamma-1)p\nabla\cdot\vec{v} + \chi\nabla^2(p-p_{eq}) + (\gamma-1)\left[\nu\rho\omega^2 + \frac{4}{3}\nu\rho(\nabla\cdot\vec{v})^2 + \eta\vec{j}\cdot(\vec{j}-\vec{j}_{eq})\right]. \quad (7)$$

Here, ρ, p, $\vec{v}$, $\vec{B}$, $\vec{E}$, $\vec{j}$ are the mass density, plasma pressure, velocity, magnetic field, electric field and current density, p_{eq}, $\vec{j}_{eq}$ are the equilibrium pressure and current, respectively. ν, η, γ, χ are viscosity, resistibility, adiabatic constant and thermal diffusion coefficient, and $\nu = \eta/\mu_0 = 10^{-5}v_aR_0$, $\chi = 10^{-7}v_aR_0$ are used for the following calculations, where v_a is the Alfvén velocity, $R_0 = 0.7$ m is the typical major radius. The time t is normalized by the Alfvén time.

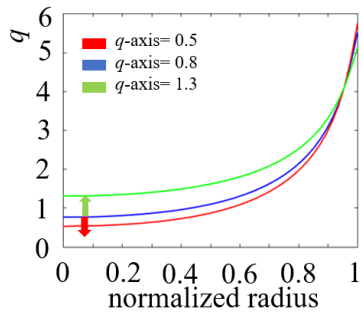

Fig. 2 q profiles of the MHD equilibria used in the MHD simulations.

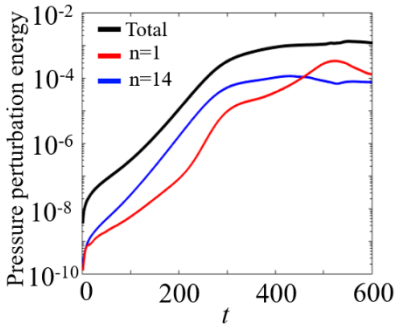

Fig. 3 Time evolutions of the pressure perturbation energy.

The MHD equilibria used in the simulations are constructed by TASK/EQ module which calculates equilibria with a fixed boundary condition. The magnetic surface of $q = 5.5$ is used for the boundary condition of the TAKS/EQ equilibrium, which corresponds to the calculation by TASK/EQU shown in Fig. 1. Figure 2 shows the q profiles of three different MHD equilibria constructed by TASK/EQ where the central beta is assumed to be $\beta_t = 2\%$. This β value is larger than the expected value $\beta_t \sim 1\%$ in the PLATO experiment, but is used to show more drastic evolutions in simulations.

Figure 3 shows the time evolution of the pressure perturbation energy for $q_{\mathrm{axis}} = 0.8$, where the pressure is normalized by B_0^2/μ_0. The total pressure perturbation energy, which is integrated for the whole plasma volume, increases monotonically in the linear phase, and show nonlinear saturation after the phase. Its Fourier decomposition to the toroidal components is also shown in Fig. 3. The initial growth rate of the $n = 1$ component is smaller than that of the $n = 14$ component, where n is the toroidal

mode number. The growth rate of the $n = 1$ component increases from $t \sim 250$ by nonlinear interaction, and becomes smaller from $t \sim 300$ in the saturation phase. Then the mode amplitude increases again from $t \sim 450$, and its magnitude becomes larger than those of the other modes. The pressure and their perturbation components in the poloidal cross-section are shown in Figs. 4 and 5, respectively. In Fig. 4 (b) and Fig. 5 (a), a ballooning mode structure whose perturbation component exists in the low field side of plasma [11,12] can be seen with finite poloidal mode numbers. Figures 6 (a) and 6 (b) show comparison of the mode spectra in the linear phase ($t = 200$) and nonlinear phase ($t = 400$). As shown in Fig. 6 (a), the dominant modes have the poloidal mode numbers of $m = 19$ around $\rho = 0.65$, where the pressure gradient is larger. Here m is the poloidal mode number. On the other hand, in the nonlinear phase in Fig. 6 (b), dominant modes exist around

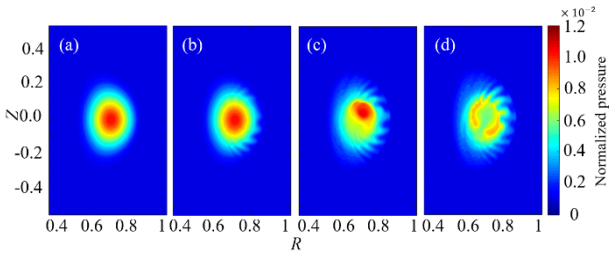

Fig. 4 Time evolution of the pressure profile in the poloidal cross-section at t = (a) 0, (b) 300, (c) 500, and (d) 600.

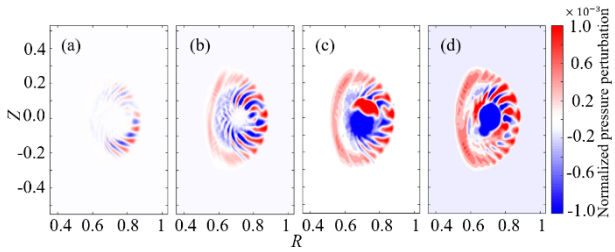

Fig. 5 Time evolution of the pressure perturbation profile in the poloidal cross-section at t = (a) 300, (b) 400, (c) 500, and (d) 600.

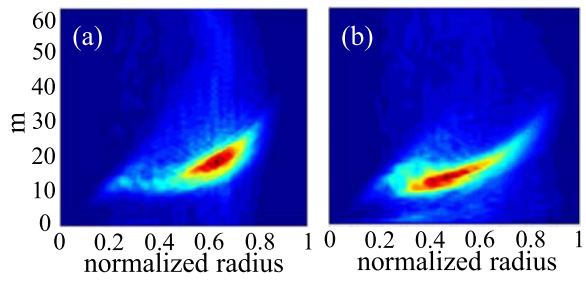

Fig. 6 Radial profiles of the mode spectrum at t = (a) 200 and (b) 400.

$\rho = 0.45$. This is because the pressure profile near $\rho = 0.65$ is flattened by the instabilities, and the steeper gradient region is shifted to the inner part near $\rho = 0.45$. In this way, the mode excited region is expanded in accordance with the flattening process. After the flattening by the ballooning modes, the $n = 1$ mode induces sudden change of the pressure profile in the central region as in Figs. 4 (c) and 4 (d). An $m/n = 1/1$ kink mode at the $q = 1$ surface [13] gives the collapse near the center. The growth rates of the $n = 1$ component at $t = 200$ and $= 450$ are almost the same, so this collapse is caused by rather linear mode growth, though some other simulation shows nonlinear excitation of a large-scale mode [6]. In this way, both of ballooning and kink modes are excited in this simulation.

4. Characteristic of the Instabilities

In this section the characteristics of the instabilities are investigated by changing plasma parameters; plasma beta, resistivity and safety factor profile. First, the dependency of the ballooning instability on the plasma beta is explained. Figure 7 shows the relation between the linear growth rate and plasma beta. The linear growth rate becomes larger, as the plasma beta is increased from 1% to 6%. Therefore, it is revealed that this instability is strengthened by the larger pressure gradient. Next, the dependency on the resistivity is examined. We carry out MHD simulations by changing η from 10^{-8} to 10^{-4}. Figure 8 shows the relation between the linear growth rate and resistivity. The linear growth rate becomes larger, as η is increased in the range $\eta > 10^{-6}$. The linear growth rate is proportional to $\eta^{1/3}$, which suggests the instability is a resistive ballooning mode in this region. Note that $\eta = 10^{-5}$ is used for the nonlinear simulation in the previous section.

In the MHD simulation in Sec. 3, both the ballooning and kink modes appear. The excited mode can be controlled by changing the q profile. Different q profiles in Fig. 2 are used as the initial conditions. Figures 9 and 10 show comparison of the time evolutions of the kinetic energy and the pressure profile with different q profiles shown in Fig. 2, respectively. In the case with $q_{\rm axis} = 1.3$, there is

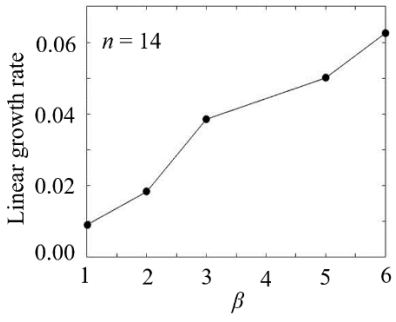

Fig. 7 Relation between the linear growth rate of the ballooning mode and β.

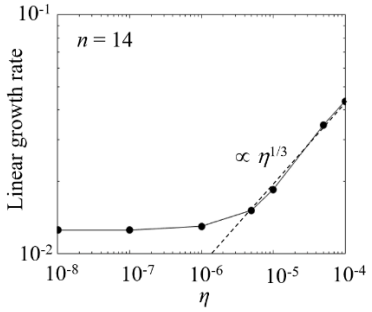

Fig. 8 Relation between the linear growth rate of the ballooning mode and η. The dashed line indicates the dependency proportional to $\eta^{1/3}$ in $\eta > 10^{-5}$.

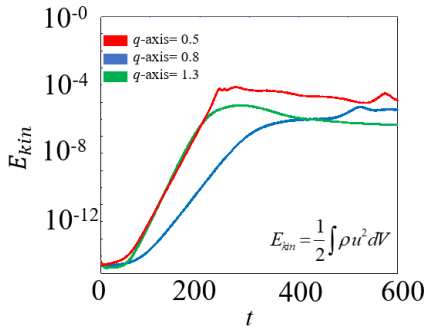

Fig. 9 Time evolution of the kinetic energy with the different q-profiles in Fig. 2.

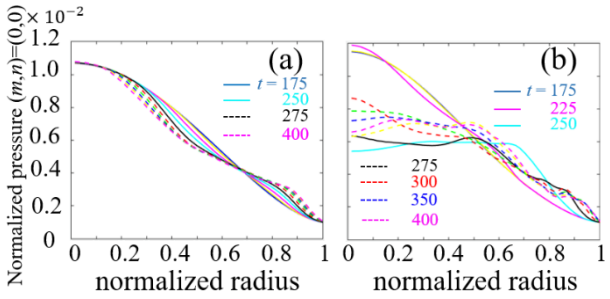

Fig. 10 Time evolutions of the pressure profile for the (a) ballooning dominant case ($q_{\rm axis} = 1.3$) and (b) kink dominant case ($q_{\rm axis} = 0.5$).

no $q = 1$ surface in the plasma, so the kink mode is not excited and the ballooning mode is dominant. When the ballooning mode is dominant, there is no sudden change in the central pressure as in Fig. 10 (a). On the other hand, in the case with $q_{\rm axis} = 0.5$, since $q_{\rm axis}$ is smaller than the case with $q_{\rm axis} = 0.8$, the kink mode is more unstable, which causes sudden change in the central pressure as shown in Fig. 10 (b). Therefore, the flattening process of the pressure profile is drastic. It is revealed that the flattening process is changed by dominant instabilities.

5. Discussion and Conclusion

In this study, the MHD simulations for PLATO plasmas were carried out for the first time by the combination of TASK and MIPS codes. The plasma equilibrium was evaluated with the vertical coil configuration of PLATO by using the free boundary equilibrium code TASK/EQU. The equilibrium was introduced into the MHD simulations and nonlinear saturation dynamics was calculated by using MIPS code. The ballooning and kink modes can both become unstable for the PLATO parameters. The parameter dependencies show their characteristics. The ballooning modes become unstable at the region with steep pressure gradient, which give rather mild flattening of the pressure profile on the low field side of the plasma. On the other hand, the kink modes with $m/n = 1/1$ become unstable near the center of the plasma, and give drastic pressure collapse of the core.

The MHD simulation shows the co-existence of ballooning and kink modes in the torus plasma. There exist several cases that include excitation of a large-scale mode by small-scale turbulence [14]. The competitive nature between the modes is examined to clarify the role in the flattening process. The effect of the dominant ballooning mode on the kink mode is explained at first. As is seen in Fig. 3, the nonlinear acceleration [15] of the $n = 1$ component is observed. There exist the modes with wide range of toroidal mode numbers, so their three-wave couplings give nonlinear energy transfer to the $n = 1$ component. In this case, the growth rate of dominant modes (e.g. $n = 13$: $\gamma_{13} = 0.019$, $n = 14$: $\gamma_{14} = 0.019$) does not satisfy the single three-wave coupling relation with that of the nonlinear accelerated mode ($n = 1$; $\gamma_1 = 0.025$), due to complex nonlinear coupling with various modes. On the other hand, a simulation with $\beta_t = 3\%$ gives the growth rates of the ballooning components much larger than that of the kink mode, and the three-wave coupling condition is almost satisfied ($\gamma_{13}(0.033) + \gamma_{14}(0.037) \sim \gamma_1(0.067)$) in the nonlinear acceleration of the $n = 1$ component. This is the case with a mode nonlinearly excited by ballooning modes, though the former one is mixture of ballooning and kink modes. Spatial structures can affect the couplings, because the excited regions of the ballooning and kink modes are different, so the effect should be investigated in detail in the future work.

Next, the effect of the ballooning mode on the dominant kink mode is explained. After the growth of the kink mode the pressure collapse expands to the outer region. Figure 11 shows radial profiles of the excited modes in the nonlinear saturation phase with the different q profiles. These are cases with and without large ballooning modes at $\rho = 0.5$ - 0.8. The magnitude of the kink mode increases, and the mode expands to the outer side, but is stopped where the ballooning modes exist, as in Fig. 11 (a). On the other hand, the mode can expand to more outer without the ballooning modes. This difference comes from the competition between the ballooning and kink modes. Detailed

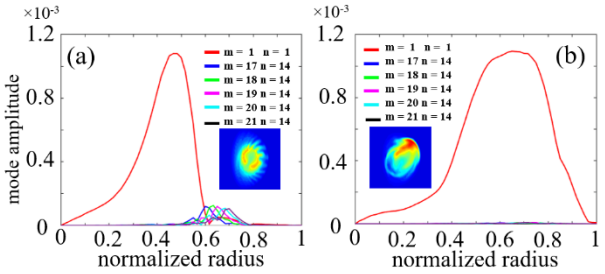

Fig. 11 Radial profiles of the excited modes in the nonlinear saturation phase. The cases with (a) competition of ballooning and kink modes (at $t = 530$ with $q_{\mathrm{axis}} = 0.8$) and (b) single kink mode (at $t = 257$ with $q_{\mathrm{axis}} = 0.5$) are shown, where the $m/n = 1/1$ mode is the kink mode.

mode interaction and spatial competition will be analyzed in the future work.

Acknowledgments

This study is partially supported by the Grant-in-Aid for Scientific Research (JP16K06938, JP17H06089, JP20K03905) of JSPS, the collaboration program of NIFS (NIFS19KNST144, NIFS18KNXN373) and of RIAM of Kyushu University. JFRS-1 supercomputer in IFERC-CSC is used for the nonlinear calculations.

[1] A.M. Dimits *et al.*, Phys. Rev. Lett. **77**, 1 (1996).
[2] R.J. Fonck *et al.*, Phys. Rev. Lett. **70**, 24 (1993).
[3] K.L. Wong *et al.*, Phys. Rev. Lett. **85**, 5 (2000).
[4] Y. Liang, Phys. Rev. Lett. **98**, 265004 (2007).
[5] P.B. Synder *et al.*, Phys. Plasmas **9**, 2037 (2002).
[6] A. Ishizawa *et al.*, Plasma Phys. Control. Fusion **61**, 054006 (2019).
[7] A. Fujisawa, AIP Conf. Proc. **1993**, 020011 (2018).
[8] http://bpsi.nucleng.kyoto-u.ac.jp/task/
[9] K. Matsuoka, Reports RIAM, Kyushu Univ. **141**, 51 (2011).
[10] Y. Todo *et al.*, Plasma Fusion Res. **5**, S2062 (2010).
[11] J.P. Freidberg, *Ideal MHD* (Cambridge University Press, 2007).
[12] J. Wesson, *Tokamaks* (Oxford University Press, 2011).
[13] M.N. Rosenbluth, R.Y. Dagazian and P.H. Rutherford, Phys. Fluids **16**, 1894 (1973).
[14] A. Ishizawa *et al.*, Phys. Plasmas **14**, 040702 (2007).
[15] M. Yagi *et al.*, Plasma Fusion Res. **2**, 025 (2007).